Phase Formation and Microstructure of Ceramics at Selective Laser Synthesis in Al_2O_3–TiO_2-Y_2O_3 Powder Compositions

M. Vlasova[*1], M. Kakazey[2], P. A. Márquez Aguilar[3], R. Guardian Tapia[4], V. Stetsenko[5], A. Bykov[6], S. Lakiza[7]

[1*]Center of Investigation in Engineering and Applied Sciences of the Autonomous University of the State of Morelos (CIICAp-UAEMor), Av. Universidad, 1001, Cuernavaca, Mexico.
[2] Frantsevich Institute for Problems of Materials Science, National Academy of Sciences of Ukraine, 3, Krzhyzhanovsky St., Kiev, 252680, Ukraine

[1*]vlasovamarina@inbox.ru; [2]kakazey@hotmail.com; [3]pmarquez@uaem.mx; [4]rene_guardian@hotmail.com; [5]stetsenkolaser@gmail.com; [6]abykov@ipms.kiev.ua; [7]sergij_lakiza@ukr.net

Abstract

Phase formation processes in the zone of directional laser irradiation of compacted Al_2O_3–TiO_2–Y_2O_3 mixtures have been investigated. It has been established that phase formation was carried out within the framework of binary systems Al_2O_3–Y_2O_3 and Y_2O_3–TiO_2. The texture of the surface of tracks and the microstructure of the obtained crystalline body depend on the ratio of the phases formed during rapid cooling of the melt and temperature distribution of the material in longitudinal and transverse directions in heating.

Keyword

Al_2O_3–Tio_2–Y_2O_3 Powder Mixtures; Laser Treatment; Phase Formation

Introduction

Laser synthesis of ceramics from powder mixtures is a promising technological method to prepare new materials with a complex of properties formed under the conditions of directional high-rate high-temperature heating and subsequent high-rate cooling. A feature of this synthesis is that phase formation occurs in a narrow band of radiation and is determined by the radiation mode, heat conduction of the material, its thermal diffusivity, and a number of other technical factors. This method called selective laser synthesis (SLS) is usually combined with selective laser sintering and selective laser melting (SLM) (Orera et al., 2000; Shishkovskii, 2009; Ester F.J. et al., 2011; Vlasova, Kakazey, Márquez Aguilar, 2011). The complexity, variety, and transience of the processes occurs in a moving zone of irradiation under conditions of rapid high-temperature heating and subsequent rapid cooling calls for the investigation of phase formation processes. This problem is most urgent when the result of irradiation is the formation of interaction products with elements of a surface texture (Vlasova et al., 2011, 2012).

The aim of this work is to investigate phase formation, the microstructure, and surface morphology in the zone of laser treatment of Al_2O_3–TiO_2–Y_2O_3 ternary powder mixtures, in which specific (local) melting and crystallization conditions are simultaneously realized.

Experimental Procedure

In the present work, specimens were prepared from analytically pure Al_2O_3, TiO_2, and Y_2O_3 powders (produced by REASOL). Powder x mol. % Al_2O_3 – y mol. % TiO_2 – z mol. % Y_2O_3 mixtures were homogenized and then compacted in pellets with a diameter of 18 mm and a thickness of 2–3 mm under a pressure of 300 MPa. The compositions of compacts are presented in Table 1. The compositions of the mixtures were calculated so that, with increase in the Al_2O_3 content in the mixtures, the TiO_2/Y_2O_3 molar ratio remained equal to 0.25.

Laser treatment was performed in the LTN-103 unit (continuous-action laser with λ = 1064 nm) in air. The power of radiation (P) was 120 W, the diameter of the beam (d) was 1.5 mm, and the linear traversing speed of the beam was v = 0.15 mm/s.

The synthesis products were investigated by the X-ray diffraction (XRD) method in Cu K_α radiation (DRON-3M, Russia). Maximum intensities (I) of diffraction lines (which are amplitudes) were registered, and the areas under the corresponding peaks were evaluated.

These areas are proportional to the contents of the corresponding crystalline phases. An electron microscopy study and microanalysis (EDS) were performed with a HU-200F type scanning electron microscope and a LEO 1450 VP unit.

Along with an investigation on the whole volume of tracks, we performed X-ray analysis of individual layers taken from the central part of tracks by removing the material of the sintering zone (the lower part) or the surface layer (see Fig. 1, d).

Results

As a result of irradiation, concave channels (tracks) were formed on the surfaces of compacted specimens (Fig. 1). Their formation is associated with the development of high temperatures in the irradiation zone, due to the melting–solidification processes proceeding simultaneously (Orera et al., 2000; Vlasova, Kakazey, Sosa Coeto, Márquez Aguilar et al., 2012). These tracks were easily removed from the compacts and analyzed as specimens. The numbers of specimens correspond to the numbers of used mixtures.

X-ray Data

It was found that concave ceramic tracks consist of $Y_3Al_5O_{12}$ (YAG), $Y_2Ti_2O_7$, and Al_2O_3 (Table I, Fig. 2), in which the YAG phase is dominant. With increment in the Al_2O_3 content in the initial mixtures ($C_{init.}$) up to 70 mol. %, the contents of all newly formed phases increase. At the same time, at $C_{init.} > 70$ mol. %, the contents of YAG and $Y_2Ti_2O_7$ decrease, whereas the corundum content continues to increase (Fig. 3, a).

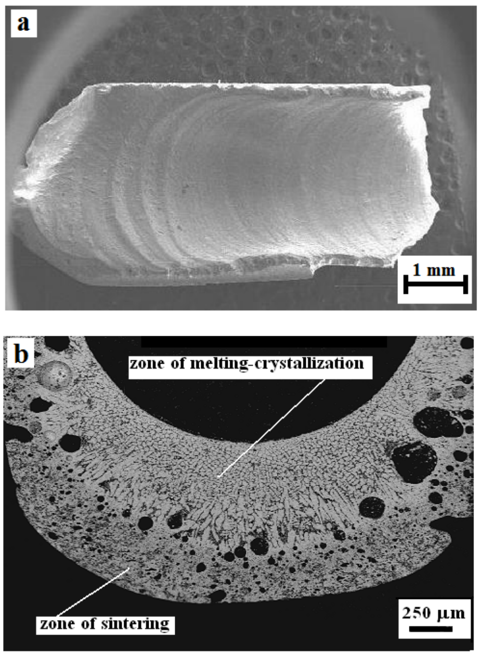

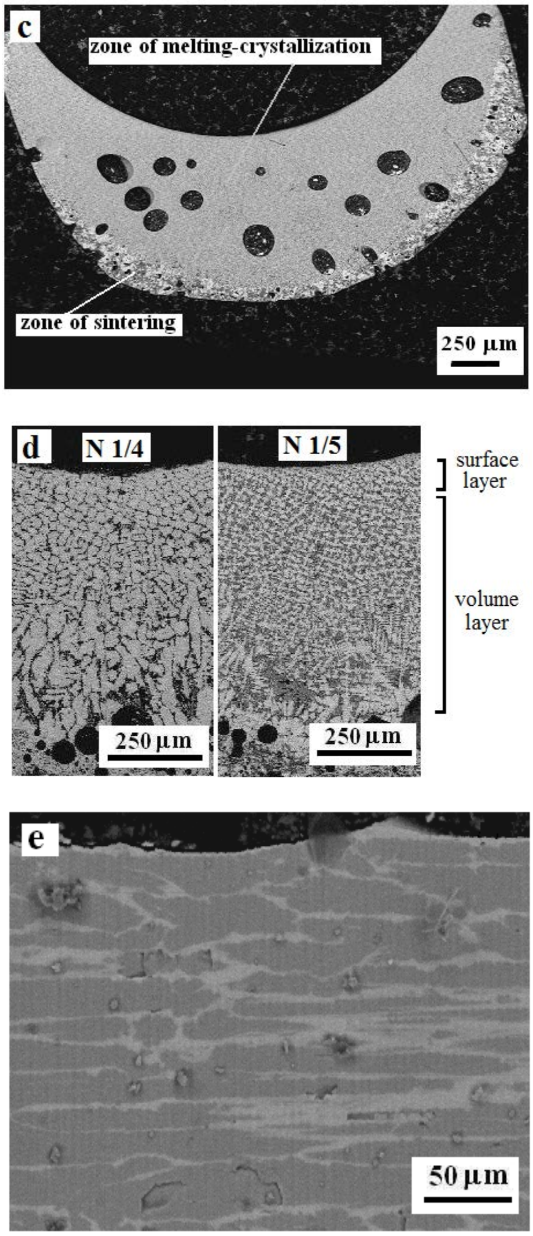

FIG. 1 ELECTRON MICROGRAPHS OF TRACKS TOP VIEW OF TRACK 1/1 (a); THE CROSS SECTION OF TRACKS 1/4 (b) AND 1/6 (c), AND LONGITUDINAL SECTION OF SURFACE LAYER OF TRACK 1/1 (e). IN (d), LAYERS TAKEN FROM THE CENTRAL PARTS OF THE TRACKS FOR XRD ANALYSIS ARE MARKED.

The deviation of the maximum intensities of the lines (amplitudes) of all phases from standard values (*JCPDS*, 1996) testifies to their texturing (see also Fig. 1 e). In Tables II–IV, texture coefficients (TC) for different phases in tracks 1/1–1/7 are presented. The calculation was performed by the formula (Ruppi, 2005).

$$TC(hkl) = \frac{I(hkl)}{I_o(hkl)} \left\{ \frac{1}{n} \sum \frac{I(hkl)}{I_o(hkl)} \right\}^{-1},$$

where I(hkl) are the measured intensities of the (hkl) reflections, I_o(hkl) are the intensities according to the JCPDS cards, and *n* is the number of reflections used in the calculation.

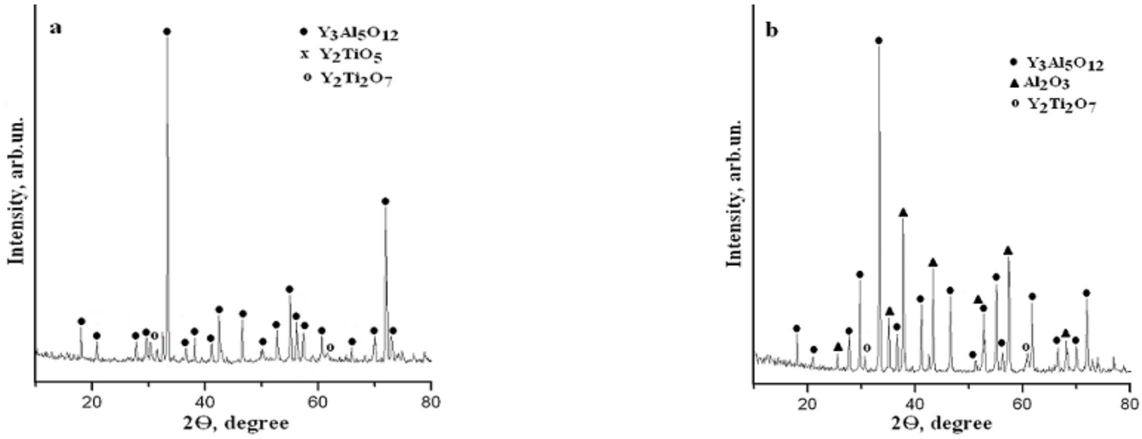

FIG. 2 FRAGMENTS OF X-RAY DIFFRACTION PATTERNS OF TRACKS (a) TRACK 1/1; (b) TRACK 1/7

TABLE I PHASE COMPOSITION IN INITIAL MIXTURES AND IN ZONE OF TRACKS

Number of Specimen	Composition of Powder Mixture			Phase Composition of Track
	Al_2O_3 , mol.%	Y_2O_3, mol.%	TiO_2, mol.%	
1/1	50	40	10	$Y_3Al_5O_{12}$, little $Y_2Ti_2O_7$, traces Y_2TiO_5
1/2	55	36	9	$Y_3Al_5O_{12}$, little $Y_2Ti_2O_7$
1/3	60	32	8	$Y_3Al_5O_{12}$, little $Y_2Ti_2O_7$, traces Al_2O_3
1/4	65	28	7	$Y_3Al_5O_{12}$, little Al_2O_3, little $Y_2Ti_2O_7$
1/5	70	24	6	$Y_3Al_5O_{12}$, Al_2O_3, little $Y_2Ti_2O_7$
1/6	75	20	5	$Y_3Al_5O_{12}$, Al_2O_3, little $Y_2Ti_2O_7$
1/7	70	16	4	$Y_3Al_5O_{12}$, Al_2O_3, little $Y_2Ti_2O_7$

TABLE II VALUES OF THE COEFFICIENTS OF TEXTURE (TC) FOR $Y_3AL_5O_{12}$ IN THE TRACKS

Phase	N track	C_{Al2O3}, mol.%	TC for <hkl>									
			<211>	<321>	<400>	<420>	<422>	<521>	<532>	<444>	<640>	<842>
$Y_3Al_5O_{12}$	1/1	50	0.34	0.39	0.29	2.18	0.27	0.76	0.65	0.72	0.96	4.5
	1/2	55	0.07	0.34	0.3	1.1	0.73	0.57	2.7	0.66	0.28	3.3
	1/3	60	0.53	0.8	0.53	1.18	0.72	1.62	0.82	0.68	1.24	1.75
	1/ 4	65	0.87	1.04	0.9	1.52	0.67	1.77	1.06	1.08	0.52	0.52
	1/5	70	0.45	1.1	1.0	1.32	0.66	1.32	1.03	0.95	0.82	1.32
	1/6	75	0.3	1.4	1.22	1.05	0.58	1.05	1.08	1.16	1.09	1.86
	1/7	80	047	0.72	0.72	0.72	1.31	1.43	0.08	0.023	1.63	1.42

TABLE III VALUES OF THE COEFFICIENTS OF TEXTURE (TC) FOR $Y_2TI_2O_7$ IN THE TRACKS

Phase	N track	C_{Al2O3}, mol.%	TC for <hkl>				
			<222>	<400>	<331>	<440>	<622>
$Y_2Ti_2O_7$	1/1	50	0.59	0.59	0.95	0.13	2.7
	1/2	55	0.13	0.83	1.03	2.26	0.77
	1/3	60	0.06	0.06	3.6	0.37	0.63

TABLE IV VALUES OF THE COEFFICIENTS OF TEXTURE (TC) FOR AL_2O_3 IN THE TRACKS

Phase	N track	C_{Al2O3}, mol.%	TC for <hkl>						
			<012>	<104>	<110>	<113>	<214>	<300>	<1010>
Al_2O_3	1/3	60	0.11	0.48	3.25	0.19	0.42	0.63	1.94
	1/4	65	0.17	0.12	0.17	0.41	0.23	0.11	5.8
	1/5	70	0.29	0.54	0.36	0.58	0.21	0.17	4.7
	1/6	75	0.49	0.78	0.51	0.76	0.13	0.27	4.0
	1/7	80	0.13	0.35	0.35	0.72	4.4	0.27	0.64

As follows from Tables II–IV, all crystalline phases carry the signs of texturing. The YAG and $Y_2Ti_2O_7$ phases have the most noticeable signs of texturing for only certain directions when the corundum content in tracks is insignificant (at $C_{init.} \leq 60$ mol. %). With increase in the corundum content in tracks, the TC for Al_2O_3 in the direction [1010] increases, and the TC for YAG in the direction [842] decreases (Fig. 3, b). For other directions, this regularity is not observed.

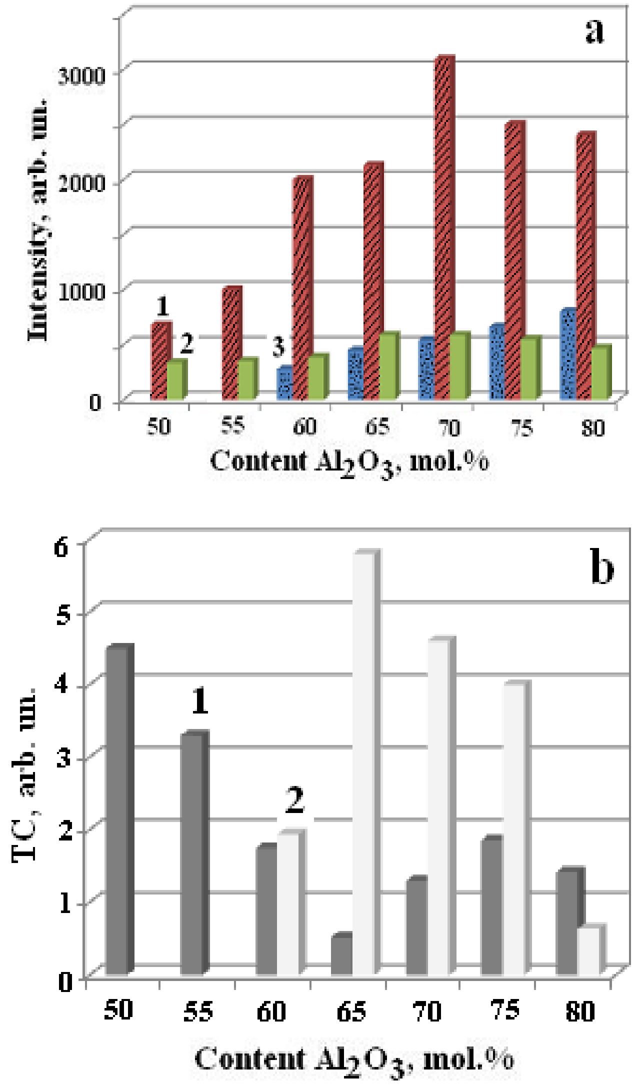

FIG. 3 CHANGE OF THE DIFFRACTION LINES INTENSITY (AREAS UNDER THE RESPECTIVE PEAKS) (a) AND TC (b) DEPENDING ON CONTENT OF Al_2O_3 IN INITIAL MIXTURES. ON a: (1) FOR THE $Y_3Al_5O_{12}$ WITH d = 0.268 nm; (2) FOR THE $Y_2Ti_2O_7$ WITH d = 0.291 nm; (3) FOR THE Al_2O_3 WITH d = 0.255 nm. ON b: (1) FOR <842> OF $Y_3Al_5O_{12}$; (2) FOR <1010> OF Al_2O_3.

It is known that the laser treatment of a ceramic surface is accompanied by its texturing (Orera, 2000). For this reason, in the present work, X-ray phase analysis on the surface and the volume layer of tracks has been carried out. The obtained data enabled us to establish two features: (1) texturing is characteristic for only surface layers; (2) texturing depends on the contents of YAG, $Y_2Ti_2O_7$, and Al_2O_3 in tracks. For instance, at large contents of YAG and $Y_2Ti_2O_7$, texturing of the surface occurs, whereas texturing of the volume layer is absent (Fig. 4, a, a′). At a large Al_2O_3 content in tracks, texturing is absent in both surface and volume layers (Fig. 4, b, b′).

SEM Data

As a result of irradiation, concave channels (tracks) formed on the surface of specimens (Fig. 1). Their formation is associated with high temperatures in the irradiation zone, due to which sintering and melting–solidification processes proceed simultaneously as the laser beam traverses the specimen surface. The tracks have a complex texture. On the surface of the tracks, a macrotexture in the form of arcs is observed, which reflects the stages of motion of the solidifying melt under the influence of the traversing laser beam (Fig. 1, a).

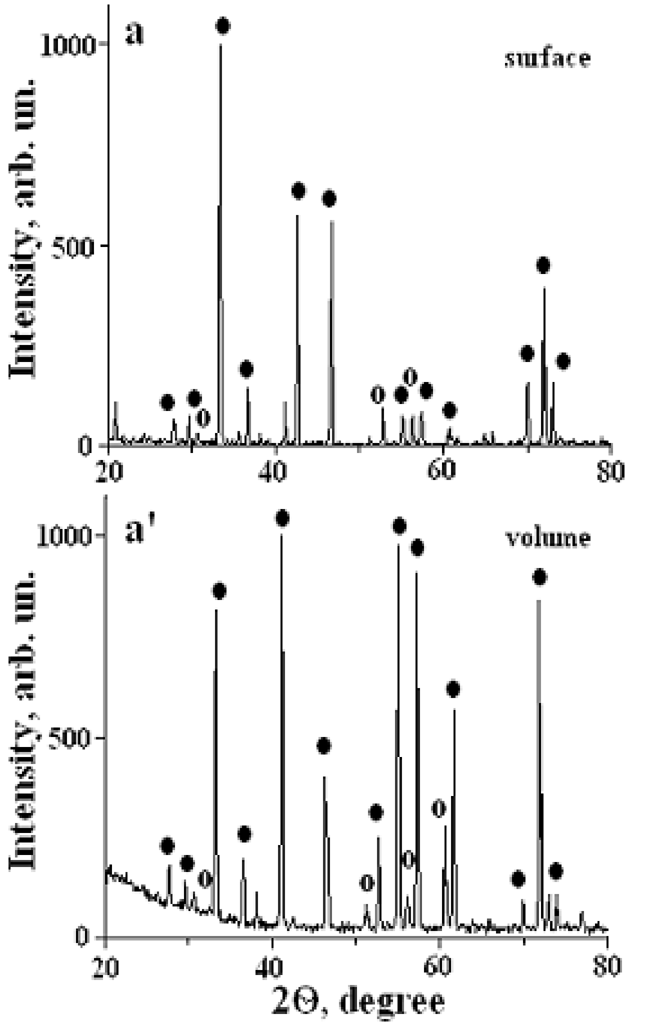

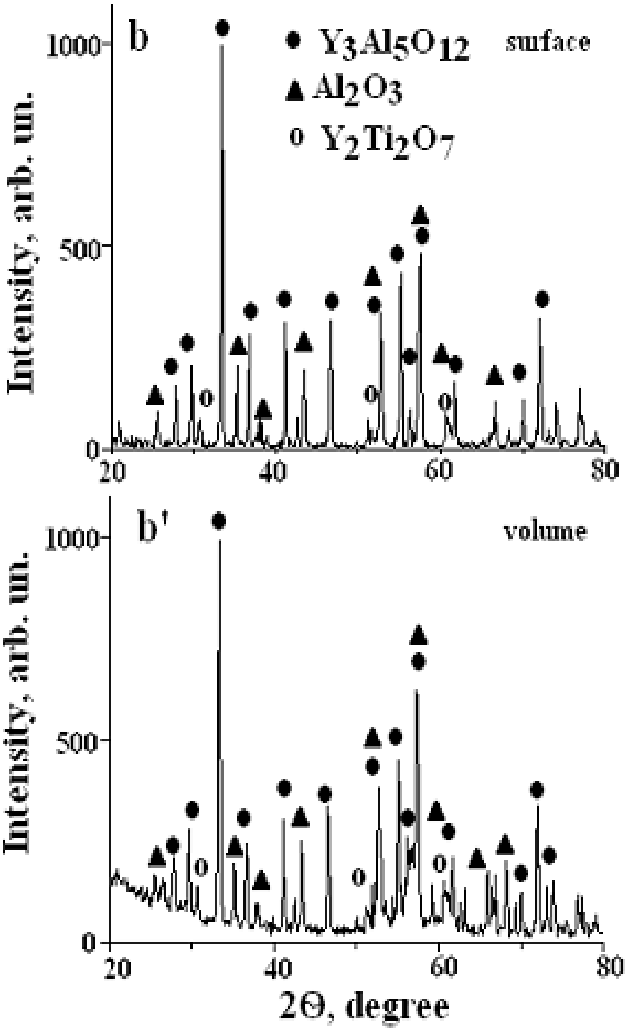

FIG. 4 FRAGMENTS OF X-RAY DIFFRACTION PATTERNS OF TRACKS (a, a') IN TRACK 1/2, (b, b') 1/6. (a, b) SURFACE LAYERS; (a', b') VOLUME LAYERS

The surface of the tracks between arcs have signs of texturing, the characteristic of which changes as the Al_2O_3 content in the tracks increases. For specimens 1/1–1/4, the surface has irregular lamellar structure (Fig. 5, a, b, c). In specimens 1/5 and 1/6, the typical longitudinal microstructure disappears (Fig. 5, d, e). The surface of specimen 1/7 (Fig. 5, f) is a faceted eutectic colony. Tracks 1/5–1/7 are characterized with the growth of (domains) lamellas in different directions.

In the cross-sections of the tracks, a melting-crystallization and a sintering zone (Fig. 1, b, c) can be easily observed. In specimens 1/1–1/5, in the melting-crystallization zone, dendrites with different sizes and orientations grow (Fig. 1, b, d). As a rule, the size of dendrites in the surface layers is smaller than that in the volume layer (see Fig. 1, d). In specimens 1/6–1/7, the indicated features of crystallization were not found.

A microstructural analysis of specimens (Fig. 6) and elemental analysis (Fig. 7) were performed on cross-sections of tracks in secondary electrons.

The microanalysis data indicate (Fig. 6, c and Fig. 7) that the elemental composition of dark gray dendrites corresponds to YAG. Light gray inclusions can be assigned to $Y_2Ti_2O_7$, and black regions are Al_2O_3.

The microstructural analysis on volume layer of samples 1/1–1/7 reveals that primary YAG crystals in samples 1/1–1/5 (Fig. 6, a-e) are clearly seen. The quantity and size of dendrites gradually increases from sample 1/1 to sample 1/4. These results also are confirmed by XRD results (Fig. 3, a). And then, in sample 1/5 the size of YAG dendrites decreases (Fig, 6, e). With a further increase in the content of the Al_2O_3 (sample 1/6 - 1/7, Fig. 6, f, g) the primary YAG crystals almost disappear. Only colonies of the two-phase eutectic Al_2O_3+YAG with the $Y_2Ti_2O_7$ traces on their boundaries are observed.

In all specimens, between primary YAG crystals, layers with different phase compositions formed. They are of eutectic nature with degeneration features. Only specimen 1/1 does not contain Al_2O_3 (Fig. 6, a), but the Al_2O_3 content increases in the following order: from specimens 1/2 to specimen 1/7 (Fig. 6, b-d, black phase). In specimen 1/5 (Fig. 6, e), the number of primary YAG crystals decreases, and almost 50% of the volume of the specimen is occupied by the Al_2O_3+YAG binary eutectic. In specimens 1/6 and 1/7, the Al_2O_3+YAG+$Y_2Ti_2O_7$ three-phase eutectic is degenerated, and detected traces of the $Y_2Ti_2O_7$ phase (see Table I) testify to its presence.

Discussion

The experimental data show that, at the chosen ratio of the initial components, YAG is predominantly formed. Yttrium titanate ($Y_2Ti_2O_7$) is present in much smaller amounts, but it was found even in the case where the contents of TiO_2 and Y_2O_3 in the mixtures were small. Taking into consideration that other ternary compounds were not detected in the specimens, it is possible to conclude that the phase formation in the irradiation zone is determined by interaction in the Al_2O_3–Y_2O_3 and Y_2O_3–TiO_2 binary systems (Fig. 8).

Under the laser radiation, a bath forms, and, after removal of the beam, crystallization begins. This is why crystallization begins from the surface, and the smallest crystals form in the surface layer. The heating temperature gradually decreases in the volume layers of the channel. For this reason, the crystallization process is retarded. However, due to the distribution of the heat of crystallization, the supercooling of the

melt is retarded. As a result, larger crystals grow and finally reach the sintering zone. In this case, crystallization in the opposite direction is also initiated. Thus, changes in the size and shape of dendrites in the vertical direction indicate the presence of certain temperature gradients, namely, the temperature is the highest on the surface and decreases in the direction to the sintering zone.

The laser beam is characterized with defocusing. In this connection, in the horizontal plane (on the surface of the specimens), a temperature gradient also takes place. Heating is most intensive at the center of the irradiated zone and less intensive in the periphery. Along with temperature diffusivity of composites and their porosity, these two temperature gradients (vertical and horizontal) are responsible for the formation of concave tracks. The difference in temperature between the heating and cooling zones of the track leads to the growth of crystallites in different directions (see Fig. 1, b).

In directed traversing of the laser beam, under the influence of hydrodynamic forces, the melt moves and is superimposed on the previous crystallized layer. As a result, arcs form on the surface of the concave track. They can be considered as a macrotexture.

The fast cooling of the moving melt is accompanied by the formation of a surface layer in the form of strands (lamellas), which can be considered as a microtextured layer. The content of Al_2O_3 crystallized from the melt affects substantially the microtexturing of the surface layer. The smaller the amount of corundum precipitated from the melt is, the more pronounced the lamellar microstructure of the surface is (see Fig. 3, a and Fig. 5, a-c). It can be concluded that, at a large content of corundum crystallites, the faster crystallization of Al_2O_3 from the melt hinders the movement of the liquid phase composed of YAG and $Y_2Ti_2O_7$.

The surface crystalline layer is characterized with the presence of crystallites textured in different directions (see Fig. 4 and Tables II-IV). It is assumed that this is connected with crystallization on the surface of the concave channel, which is eventually determined by both two temperature gradients and the content of the liquid melt composed of YAG and $Y_2Ti_2O_7$. The less the content of these phases is, the smaller the TC for the compounds YAG and $Y_2Ti_2O_7$ is (see Fig. 3). In this case, the difference in texturing of the surface and volume layers gradually disappears. For the Al_2O_3 phase, the TC increases only to a certain corundum content, namely, in tracks 1/3 and 1/5.

The evolution of the microstructure of the ceramic tracks is set by the content of corundum crystallites precipitated from the melt. Their content, in turn, depends on the content of Al_2O_3 in the initial mixtures. In the case where the Al_2O_3 content in the initial mixtures is less than 54 mol. % and does not exceed ~ 48 mol. %, the track consists of YAG primary crystals with layers containing small amounts of $Y_2Ti_2O_7$ and Y_2TiO_5 (Fig. 6, a, Table 1). If $C_{init.}$ ~ (54–70) mol.%, the composition of tracks corresponds to the region of YAG primary crystallization with thin layers of the degenerated YAG + $Y_2Ti_2O_7$ and YAG + Al_2O_3 two-phase eutectics and Al_2O_3+ $Y_2Ti_2O_7$+ YAG three-phase eutectic (Fig. 6, b–e). If the Al_2O_3 content in the initial mixtures exceeds ~ 75 mol. %, tracks contain small primary Al_2O_3 crystals, large areas of the Al_2O_3+YAG binary eutectic and small degenerated areas of the same Al_2O_3+$Y_2Ti_2O_7$+YAG three-phase eutectic (Fig. 6, f, g). It should be noted that the quantity of the ternary eutectic is very small, and it is not clearly seen in the presented figures, but, according to the laws of construction of phase diagrams, it must be present.

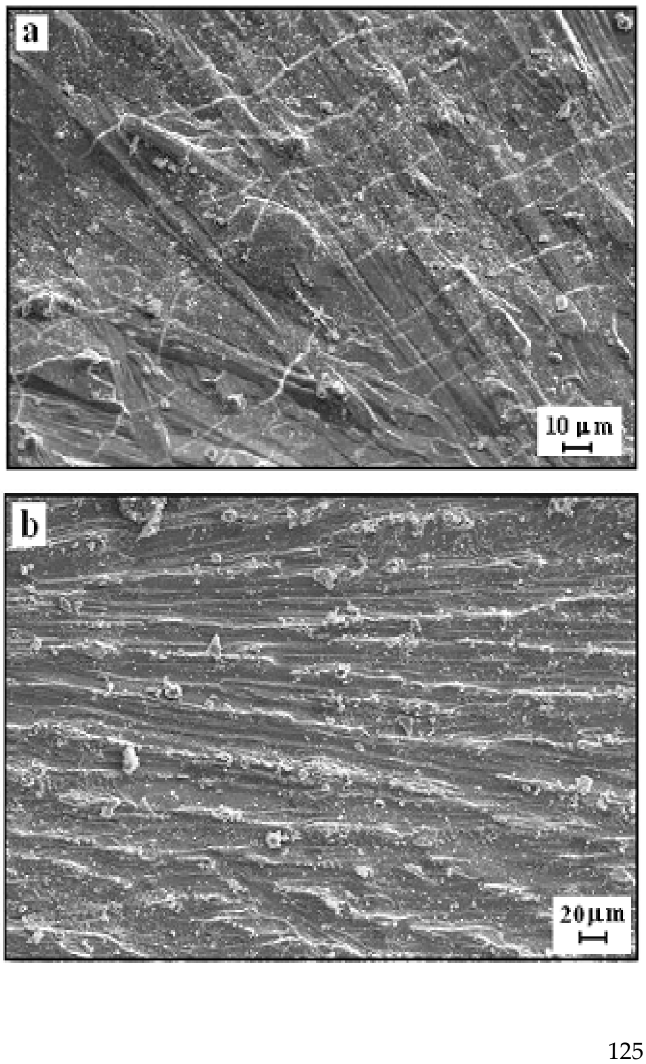

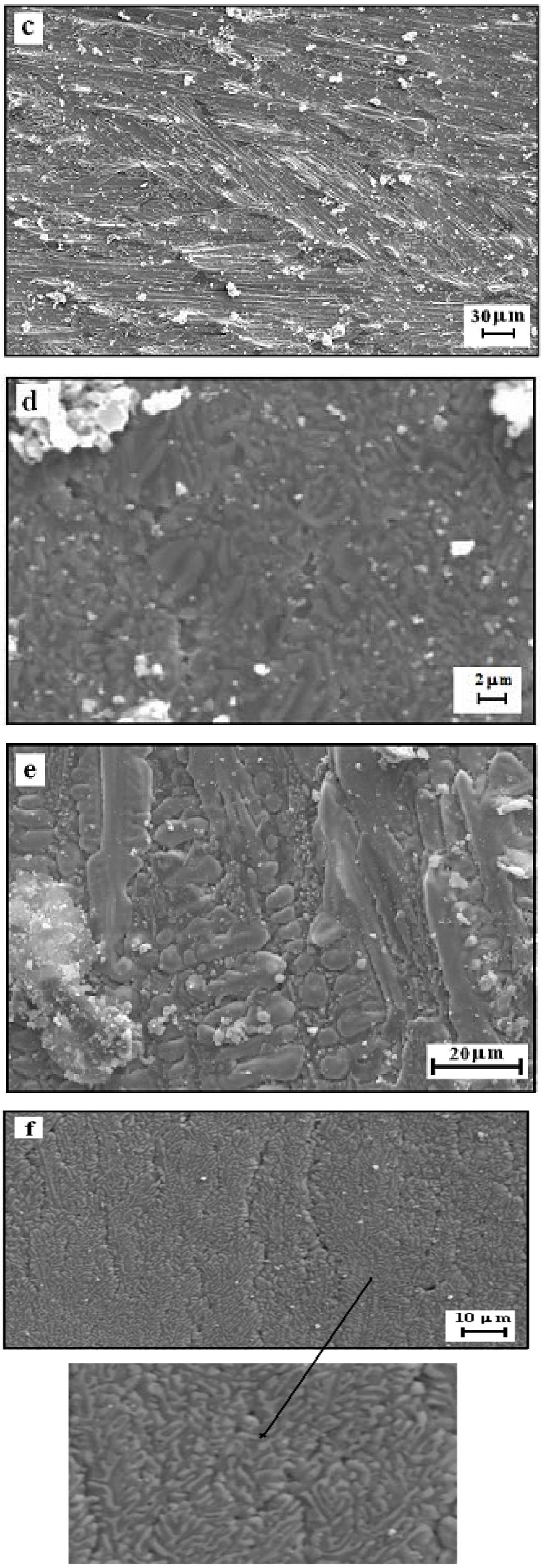

FIG. 5 ELECTRON MICROGRAPHS OF THE SURFACE OF TRACKS 1/1 (a), 1/3 (b), 1/4 (c), 1/5 (d), 1/6 (e), 1/7 (f)

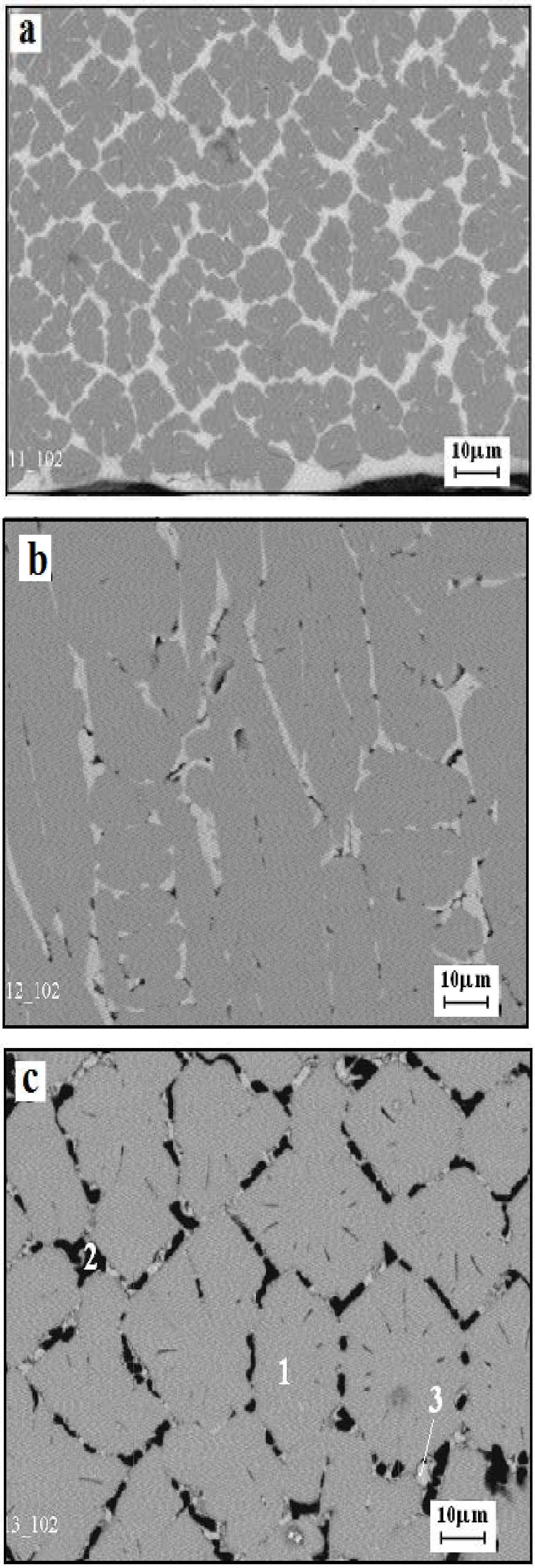

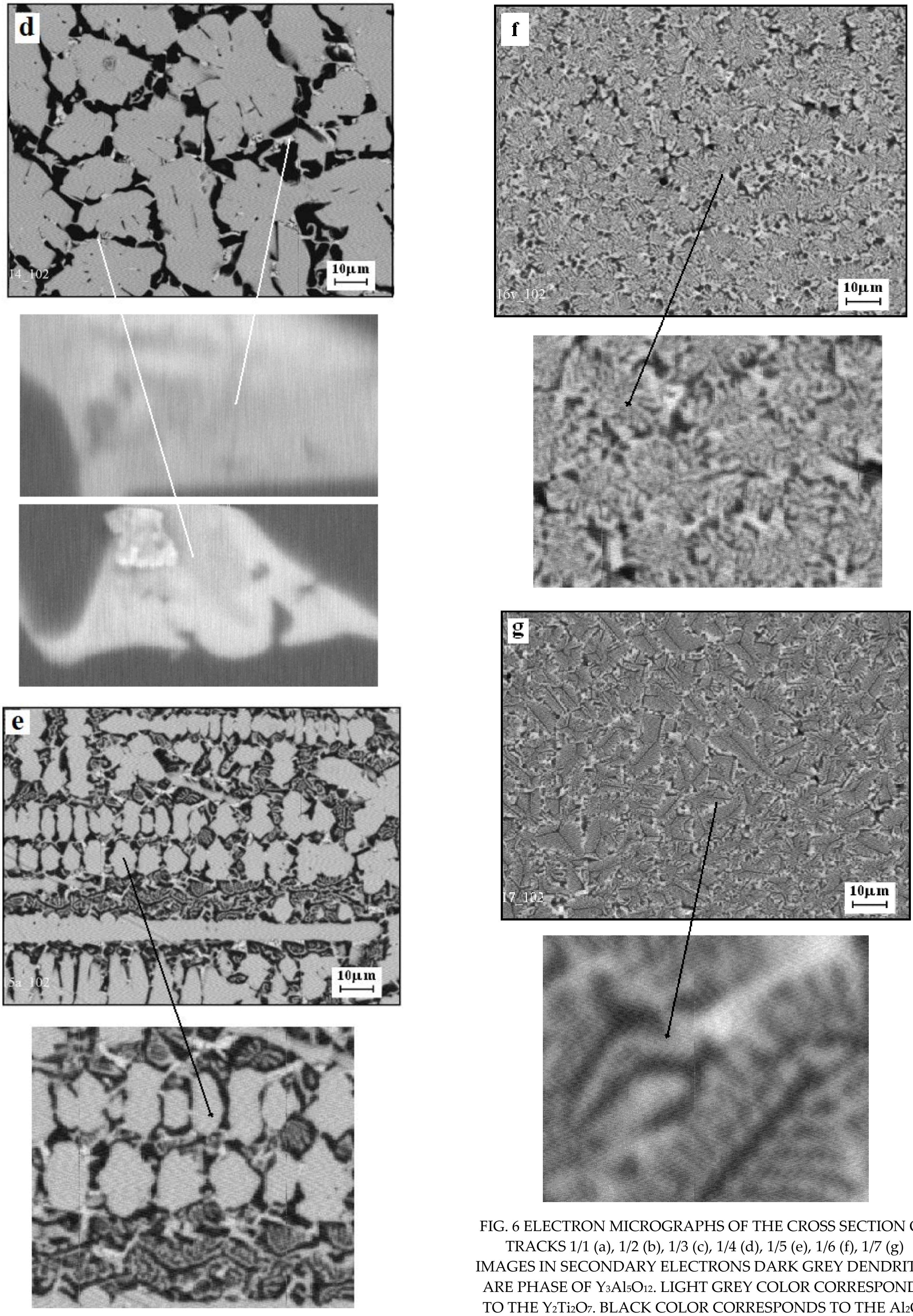

FIG. 6 ELECTRON MICROGRAPHS OF THE CROSS SECTION OF TRACKS 1/1 (a), 1/2 (b), 1/3 (c), 1/4 (d), 1/5 (e), 1/6 (f), 1/7 (g) IMAGES IN SECONDARY ELECTRONS DARK GREY DENDRITES ARE PHASE OF $Y_3Al_5O_{12}$. LIGHT GREY COLOR CORRESPONDS TO THE $Y_2Ti_2O_7$. BLACK COLOR CORRESPONDS TO THE Al_2O_3

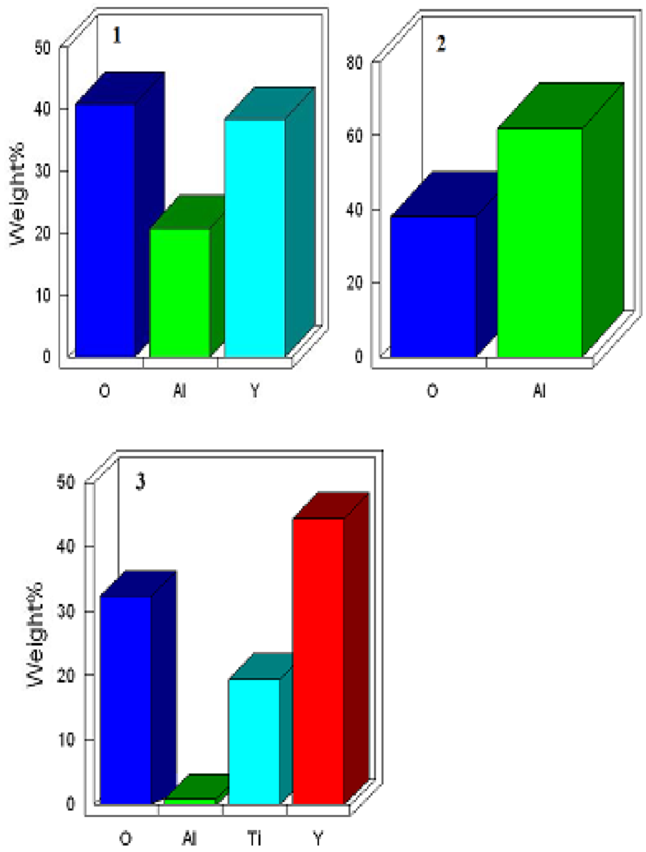

FIG. 7 CONTENTS OF ELEMENTS AT DIFFERENT PLACES OF THE SURFACE OF TRACK 1/3. 1, 2, 3 CORRESPOND TO PLACES 1, 2, 3 IN FIG. 6 c.

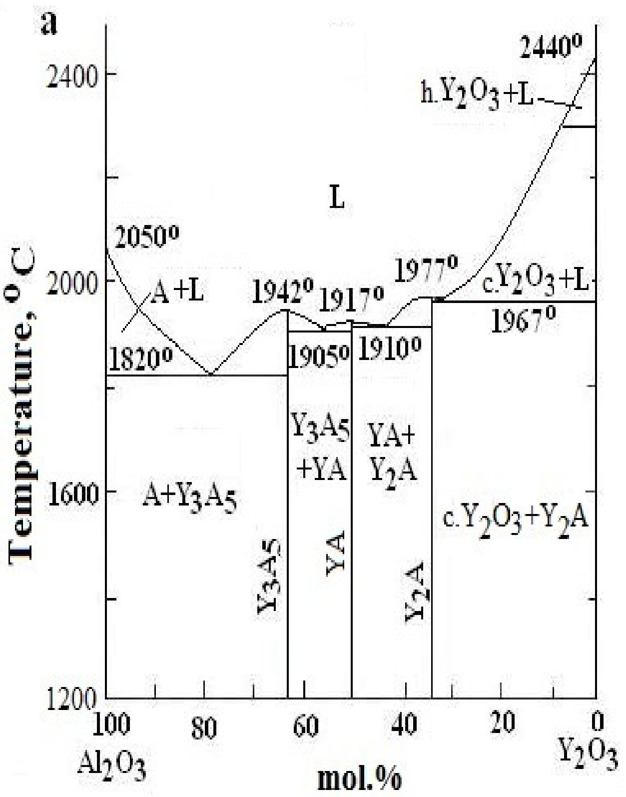

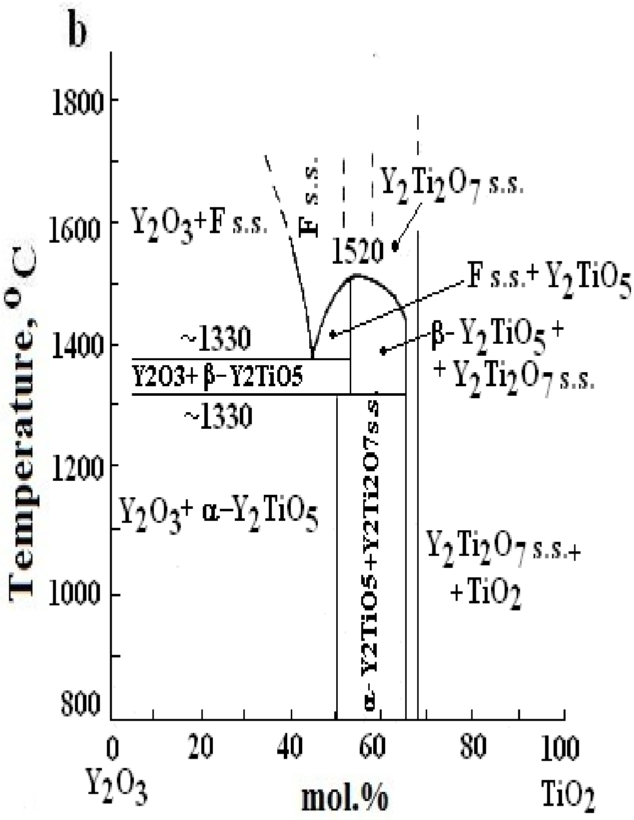

FIG. 8 THE PHASE DIAGRAMS OF Al_2O_3-Y_2O_3 AND Y_2O_3-TiO_2 SYSTEMS. DESIGNATIONS: Al_2O_3 (A), $YAlO_3$ (YA), $Y_3Al_{15}O_{12}$ (Y_3A_5), $Y_4Al_2O_9$ (Y_2A), LIQUID STATE (L), (C.) CUBIC, (H.) HEXAGONAL, SOLID SOLUTION (S.S.), FLUORITE-TYPE (F) (TOROPOV, 1969).

Conclusions

The performed investigations on laser irradiation of x mol. % Al_2O_3 – y mol. % TiO_2 – z mol. % Y_2O_3 mixtures at TiO_2/Y_2O_3 = 0.25 showed the following:

ternary compounds were not detected in the specimens, and, therefore, phase formation occurred within the framework of the Al_2O_3–Y_2O_3 and Y_2O_3–TiO_2 binary compounds and accompanied by the formation of YAG, $Y_2Ti_2O_7$, and an excess of Al_2O_3;

The texture of the surface layers of tracks and the microstructure of obtained crystalline bodies depend on the ratio of the phases formed during rapid cooling of the melt; the macro- and the microstructure of specimens is affected by the temperature distribution in the material in the longitudinal and transverse directions in heating.

ACKNOWLEDGMENT

The authors wish to thank CONACYT for financial support (Project 155731).

REFERENCES

Ester F. J., Larrea A., Merino R. I., “Processing and microstructural study of surface laser remelted Al_2O_3-YSZ-YAG eutectic plates”, J. European Ceram. Soc. vol. 31(7), pp. 1257-1268, 2011.

JCPDS, Swarthmore, PA, 1996.

Orera V. M., Merino R. I., Pardo J. A., Larrea A. A., Peña J. I., Gonzalez C., Poza P., Pastor J. Y., Llorca J., “Microstructure and physical properties of some oxide eutectic composites processed by directional solidification”, Acta Mater., vol. 48 (18/19), pp. 4683–4689, 2000.

Ruppi S., “Deposition, microstructure and properties if texture-controlled CVD α-Al_2O_3 coatings”, Int. J. Refract. Met. Hard Mater. vol. 23 (4–6), pp. 306–316, 2005.

Shishkovskii V., Laser synthesis of functional mesostructures and 3D parts, Ed. Moscow, Russia: Fizmatlit, 2009.

Toropov N. A., Phase diagrams of silicate systems, Ed. Leningrad, Russia, Nauka, 1969.

Vlasova M., Kakazey M., Márquez Aguilar P. A., in: Advances in ceramics. Synthesis and characterization, processing and specific application, Ed. Costas Sikalidis, INTECH, Open Access Publisher, 2011.pp.393-420.

Vlasova M., Kakazey M., Marquez Aguilar P. A., Guardian Tapia R., Juarez Arellano E., Stetsenko V., Ragulya A., Bykov A., Timofeeva I., “Peculiarities of Ruby Synthesized from Al_2O_3–Cr_2O_3 Powder Mixture by Selective Laser Sintering”, J. Laser Micro/ Nanoengineering, vol. 6, No.2, pp.96-104, 2011.

Vlasova M., Kakazey M., Sosa Coeto B., Marquez Aguilar P. A., Rosales I., Escobar Martinez A., Stetsenko V., Bykov A., Ragulya A., “Laser Synthesis of Al_2TiO_5 and $Y_3Al_5O_{12}$ Ceramics from Powder Mixtures Al_2O_3-TiO_2 and Al_2O_3-Y_2O_3”, Sci.Sintering, vol. 44, (2), pp.17-24, 2012.

Vlasova M., Kakazey M., Sosa Coeto B., Rosales I., Márquez Aguilar P. A., Stetsenko V., Bykov A., “Phase formation in zone of laser irradiation of Al_2O_3-TiO_2-Y_2O_3 powder mixtures”, in Proc. XXXIII Encuentr Nacional y II Congreso Internacional AMIDIQ, Mexico, pp.1409-1414, 2012.